

Partially Oxidized  $Ti_3C_2T_x$  MXenes for Fast and Selective Detection of Organic Vapors at Part-per-Million Concentrations

Hanna Pazniak,\* Ilya A. Plugin, Michael J. Loes, Talgat M. Inerbaev, Igor N. Burmistrov, Michail Gorshenkov, Josef Polcak, Alexey S. Varezchnikov, Martin Sommer, Denis V. Kuznetsov, Michael Bruns, Fedor S. Fedorov, Nataliia S. Vorobeva, Alexander Sinitskii,\* and Victor V. Sysoev\*

Cite This: *ACS Appl. Nano Mater.* 2020, 3, 3195–3204

Read Online

ACCESS |

Metrics & More

Article Recommendations

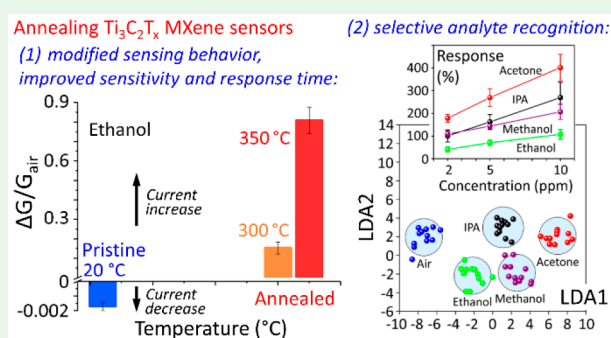
Supporting Information

**ABSTRACT:** MXenes, two-dimensional transition metal carbides or nitrides, have recently shown great promise for gas sensing applications. We demonstrate that the sensitivity of intrinsically metallic  $Ti_3C_2T_x$  MXene can be considerably improved via its partial oxidation in air at 350 °C. The annealed films of MXene sheets remain electrically conductive, while their decoration with semiconducting  $TiO_2$  considerably improves their chemiresistive response to organic analytes at low-ppm concentrations in dry air, which was used to emulate practical sensing environments. We demonstrate that partially oxidized MXene has a faster and a qualitatively different sensor response to volatile analytes compared to pristine  $Ti_3C_2T_x$ . We fabricated multisensor arrays of partially oxidized  $Ti_3C_2T_x$  MXene devices and demonstrate that in addition to their high sensitivity they enable a selective recognition of analytes of nearly the same chemical nature, such as low molecular weight alcohols. We investigated the oxidation behavior of  $Ti_3C_2T_x$  in air in a wide temperature range and discuss the mechanism of sensor response of partially oxidized MXene films, which is qualitatively different from that of pristine  $Ti_3C_2T_x$ .

**KEYWORDS:** MXene, titanium carbide, gas sensor, multisensor array, chemiresistive response, titanium dioxide, work function

## INTRODUCTION

Because of their extremely high surface-to-volume ratio, very diverse chemical and electronic properties, and integrability with planar electronic devices, two-dimensional (2D) materials are widely regarded as promising candidates for highly sensitive gas sensors.<sup>1</sup> Following the demonstration of single-molecule sensitivity in graphene,<sup>2</sup> a variety of 2D nanostructures based on graphene-based materials,<sup>3–5</sup> transition metal dichalcogenides,<sup>6,7</sup> phosphorene,<sup>8</sup> and layered semiconducting oxides<sup>9</sup> have been extensively tested in sensor experiments. Recent studies suggest that MXenes, a new class of 2D materials, also show a great promise for gas sensing applications.<sup>10–17</sup> MXenes are transition metal carbides/nitrides with a general formula of  $M_{n+1}X_nT_x$  ( $n = 1, 2, \text{ or } 3$ ), where  $M$  stands for an early transition metal,  $X$  is C or N, and  $T_x$  represents surface functional groups, mostly  $-F$ ,  $-O$ , and  $-OH$ .<sup>18</sup> In general, MXenes are synthesized by removing the A-element (Al or Si) from the bulk MAX phase precursor via selective chemical etching.<sup>19</sup> The functional groups ( $-F$ ,  $-O$ , and  $-OH$ ) on the MXene surface can serve as abundant active sites to facilitate gas adsorption and charge transfer. First-principles simulations showed that oxygen-terminated MXenes of  $M_2C$  type, where  $M$  is Sc, Ti, Zr, or Hf, could be sensitive to ammonia.<sup>10,11</sup> Experimental efforts so far have been focused on



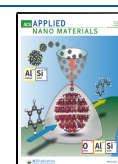
the investigation of sensing properties of  $Ti_3C_2T_x$ , the most studied MXene material to date, which was shown to be sensitive to low concentrations of acetone, ethanol, methanol, and ammonia vapors at room temperature.<sup>12–17</sup> Noteworthy, while  $Ti_3C_2T_x$  is a metallic conductor<sup>20</sup> and in the previous sensor studies the  $Ti_3C_2T_x$  MXene sheets exhibited a metallic behavior, considerably higher chemiresistive responses to organic vapors are generally known for semiconducting oxide nanostructures.<sup>21</sup> The latest studies show that  $Ti_3C_2T_x/TiO_2$  nanocomposites can be used as chemiresistors with enhanced responses to ammonia at ppm concentrations<sup>22</sup> and as humidity sensors of chemicapacitor type.<sup>23</sup> In both cases, the responses of nanostructured materials were higher than those of pristine  $Ti_3C_2T_x$ .

In this study, we demonstrate that the already impressive properties of  $Ti_3C_2T_x$ -based sensors can be further improved

Received: November 16, 2019

Accepted: March 20, 2020

Published: March 20, 2020



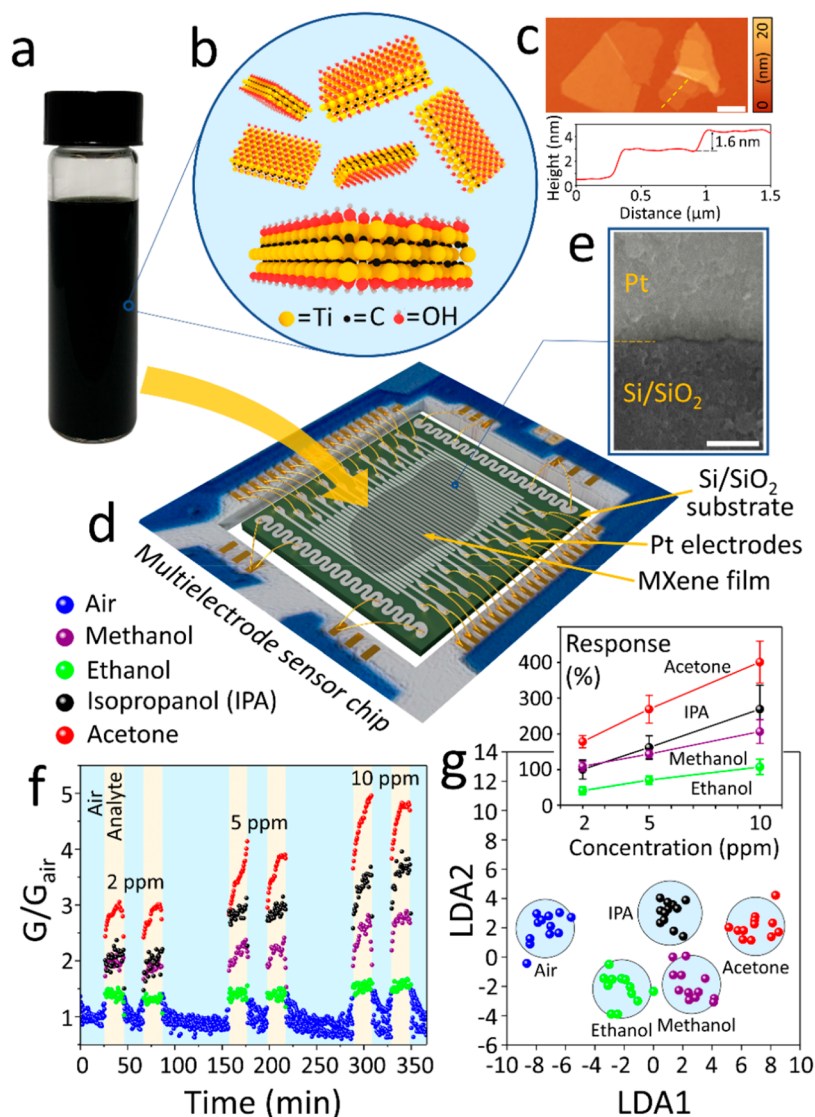


**Figure 1.** Gas sensing properties of a partially oxidized  $\text{Ti}_3\text{C}_2\text{T}_x$  MXene film on a multisensor chip. (a) Photograph of a stable delaminated MXene solution in water. (b) The schematic structure of monolayer  $\text{Ti}_3\text{C}_2\text{T}_x$  MXene flakes. (c) AFM image of  $\text{Ti}_3\text{C}_2\text{T}_x$  MXene flakes on  $\text{Si}/\text{SiO}_2$ . Scale bar is  $1 \mu\text{m}$ . The bottom panel shows the height profile measured across two MXene monolayers along the dashed yellow line in the AFM image. (d) Scheme of a multisensor chip with a film of MXene flakes prepared by drop-casting. (e) SEM image of a MXene film covering the contact area between the Pt electrode and  $\text{Si}/\text{SiO}_2$  substrate. Scale bar is  $1 \mu\text{m}$ . (f) The MXene local conductance  $G(t)$  variation of a representative chemiresistive element between two adjacent Pt electrodes on the multisensor chip in dry air under sequential dosing of acetone, isopropyl alcohol (IPA), ethanol, and methanol at 2–10 ppm concentrations relative to the conductance in air,  $G_{\text{air}}$ . The sensing experiments were performed at  $350 \text{ }^\circ\text{C}$ . (g) Inset: Dependence of the chemiresistive response,  $S = \Delta G/G_{\text{air}}$ , averaged for all MXene sensing elements on a chip on the organic vapor concentration; the error bars indicate the resistance fluctuations over the entire multisensor array. Main panel: Multisensor array vector signals for three organic vapors (10 ppm) and dry air projected by LDA into a two-component discrimination diagram; the gas-related circles are built with a 0.7 confidence around the corresponding gravity centers.

by their annealing in air at around  $350 \text{ }^\circ\text{C}$ , resulting in a partial surface oxidation. The annealed films of MXene sheets remain electrically conductive, while their decoration with semiconducting  $\text{TiO}_2$  considerably improves their sensor chemiresistive response to organic vapors at low-ppm concentrations. In addition to showing higher sensitivity, the partially oxidized MXene responds to volatile analytes faster than pristine  $\text{Ti}_3\text{C}_2\text{T}_x$ . Also, unlike previous studies of MXene-based sensors, in which the experiments were primarily performed using nitrogen as a background, we performed our measurements in dry air to emulate practical sensing environments. We also demonstrate that the sensing responses of pristine and partially oxidized MXene films are qualitatively different: in the

presence of alcohol molecules the electrical conductivity decreases for pristine  $\text{Ti}_3\text{C}_2\text{T}_x$  but increases for the partially oxidized material, which we attribute to the effect of semiconducting  $\text{TiO}_2$  nanoparticles. The experimental data shed light on the charge carrier exchange at the  $\text{TiO}_2/\text{MXene}$  interface that facilitates the remarkable gas-sensor properties of this material. Furthermore, while previous experimental studies of MXene-based sensors primarily focused on establishing their sensitivity limits,<sup>12–14</sup> here we also discuss their potential for highly selective analyte recognition and demonstrate that partially oxidized  $\text{Ti}_3\text{C}_2\text{T}_x$  MXene films can be integrated into multisensor arrays capable of reliable discrimination of very similar organic molecules, such as low molecular weight

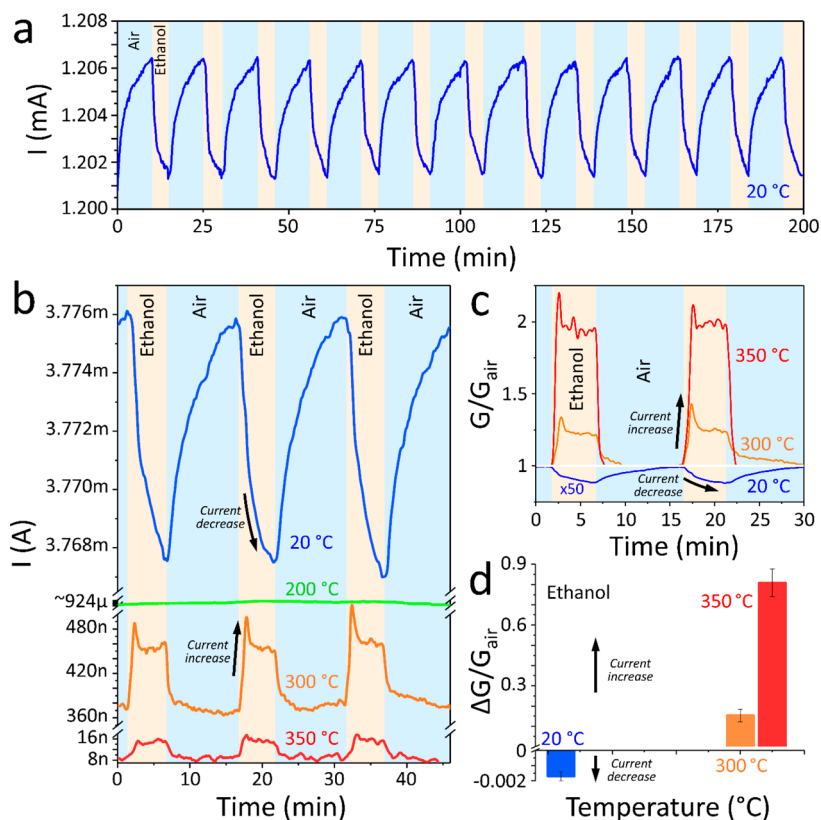


**Figure 2.** Sensor behavior of  $\text{Ti}_3\text{C}_2\text{T}_x$  MXene annealed at different temperatures. All panels show sensor responses to 250 ppm of ethanol. The voltage applied between the device contacts was 1 V. (a) Stability of sensor responses of pristine  $\text{Ti}_3\text{C}_2\text{T}_x$  MXene measured at room temperature (20 °C). (b) Responses of a MXene sensor element that was measured at room temperature (20 °C; blue curve) and then annealed at 200 °C (green curve), 300 °C (orange curve), and 350 °C (red curve). After each annealing the sensor measurements were performed at the annealing temperature. (c) Normalized sensor responses at different temperatures for the same MXene sensor element. The responses for the pristine metallic MXene are multiplied by 50 to be visible on the figure scale. (d) Comparison of sensor responses at different temperatures for the same MXene sensor element.

alcohols. Importantly, low-ppm sensitivity and analyte discrimination were achieved not in an inert environment, such as nitrogen, but in dry air, demonstrating the potential of partially oxidized  $\text{Ti}_3\text{C}_2\text{T}_x$  MXene for practical applications, particularly in healthcare.<sup>24</sup> The superior sensitivity and selectivity characteristics of gas sensors based on partially oxidized  $\text{Ti}_3\text{C}_2\text{T}_x$  MXene films warrant further investigation of sensing properties of other MXene/metal oxide hybrid structures.

## RESULTS AND DISCUSSION

We synthesized  $\text{Ti}_3\text{C}_2\text{T}_x$  MXene by the minimally intensive layer delamination (MILD) method<sup>25</sup> by etching Al from  $\text{Ti}_3\text{AlC}_2$  MAX phase (Figure S1) using the *in situ* formation of hydrofluoric acid, as detailed in the Experimental Section. The method produced an aqueous solution of well-dispersed  $\text{Ti}_3\text{C}_2\text{T}_x$  MXene sheets (Figure 1a) that are schematically shown in Figure 1b. A representative atomic force microscopy (AFM) image of  $\text{Ti}_3\text{C}_2\text{T}_x$  deposited on a Si/SiO<sub>2</sub> substrate shows uniform, well-exfoliated MXene flakes that are few micrometers in size (Figure 1c). The steps in the AFM height profile measurement indicate individual MXene monolayers, one lying on top of the other. The top step height of about 1.6 nm corresponds to the previously reported AFM-measured thickness of a  $\text{Ti}_3\text{C}_2\text{T}_x$  monolayer; the bottom layer appears to be thicker due to the presence of adsorbate molecules at the interface with the Si/SiO<sub>2</sub> substrate; see ref 26 for details.

For the gas sensing measurements, we first drop-casted an aqueous  $\text{Ti}_3\text{C}_2\text{T}_x$  solution (Figure 1a) on a multielectrode chip, which dried forming a uniform multilayer film of MXene flakes (Figure 1d). Figure 1e shows a top-view scanning electron microscopy (SEM) image of the MXene film, in which the overlapping flakes in a continuous film are difficult to distinguish. The multielectrode chips were equipped with thermoresistors and heaters (all made of Pt, 1 μm thick) on a Si/SiO<sub>2</sub> substrate, as described in the Experimental Section. Each pair of Pt electrodes bridged by the  $\text{Ti}_3\text{C}_2\text{T}_x$  film constituted a single chemiresistive element that could be measured independently of other elements (Figure 1d). The entire multisensor array comprised 38 MXene sensor elements (Figure 1d).

Prior to the sensor measurements, the MXene film on the multielectrode chip was first partially oxidized by annealing in air at about 350 °C for 24 h using the built-in heaters. The rationale for selecting the annealing temperature is discussed below and was based on the systematic analysis of gas sensing properties of MXene films annealed at different temperatures. The selection of this temperature was further supported by the results of thermal analysis, which showed that 350 °C is the onset of active oxidation of  $\text{Ti}_3\text{C}_2\text{T}_x$ , at which most of the MXene material survives while a noticeable amount of semiconducting TiO<sub>2</sub> forms enhancing the gas sensing properties. During the sensing experiments we measured the conductance of different MXene sensor elements on the

multielectrode chip while it was exposed in a flow mode to dry air mixed with an organic vapor (acetone, methanol, ethanol, or isopropyl alcohol) at low ppm concentrations; see [Experimental Section](#) for details. We found that the optimum operating temperature to facilitate the chemiresistive effect was also about 350 °C, which was the highest available for the chip. Under heating, the conductance of the partially oxidized MXene film was significantly enhanced in the presence of organic vapors with reproducible recovery under dry air, as shown in [Figure 1f](#). The characteristic responses were on the time scale of minutes, which was largely related to the rate of the gas delivery in the experimental gas-mixing setup. The chemiresistive response ( $S$ ) calculated as a change of conductance divided by its value in dry air follows almost a linear dependence on the vapor concentration ( $C$ ) in the 2–10 ppm range (see the inset in [Figure 1g](#)) in accordance with the Freundlich isotherm,  $S \sim C^\alpha$ , where  $\alpha$  is close to 1. At the lowest tested vapor concentration of 2 ppm the observed response values were 40% (ethanol), 110% (methanol), 100% (isopropyl alcohol), and 180% (acetone) enabling reliable gas detection. By linear extrapolation of the  $S(C)$  dependence to the lower gas concentration range where the response is 10% as detailed in [ref 27](#), the corresponding detection limits for these test vapors were estimated to be about 150, 35, 40, and 20 ppb, respectively. The superior sensing properties of the oxidized MXene films are illustrated in the Supporting Information ([Figure S2](#)), where they are compared to those of pristine  $\text{Ti}_3\text{C}_2\text{T}_x$ <sup>14</sup> and other recently reported MXene-TiO<sub>2</sub> hybrids.<sup>22,23</sup> Noteworthy, in previous sensor measurements of pristine  $\text{Ti}_3\text{C}_2\text{T}_x$  the gas molecules adsorbed on a device channel always increased its resistance relative to nitrogen background regardless of whether they had donor or acceptor properties, which was attributed to the metallic conductivity of  $\text{Ti}_3\text{C}_2\text{T}_x$ .<sup>14</sup> Here, the partially oxidized MXene sheets exhibited a reduction of resistance when exposed to reducing gases similar to the behavior of oxide chemiresistors, which further suggests the importance of semiconducting TiO<sub>2</sub> in the observed sensing behavior. A similar change in the gas sensing response was recently observed upon decoration of  $\text{Ti}_3\text{C}_2\text{T}_x$  with semiconducting WSe<sub>2</sub>.<sup>28</sup>

Since all tested molecules affect the charge transport in devices based on the partially oxidized MXene in a similar way by reducing their resistance, it is difficult to discriminate these analytes using a single sensor element. Achieving high selectivity in analyte recognition is also an apparent challenge for MXene-based sensors with metallic conductivity due to the comparable effects on conductance of adsorbed molecules, regardless of their donor or acceptor properties.<sup>14</sup> Here we demonstrate that highly selective gas recognition can be achieved by integrating devices in a multisensor array ([Figure 1d](#)) and processing the vector signals from all sensors on a chip using linear discriminant analysis (LDA).<sup>29–31</sup> The illustrative planar diagram representing the resulting LDA space is shown in [Figure 1g](#). The data clusters corresponding to the vector signals from different gases built at the confidence probability of 0.7 are well separated with a Mahalanobis distance<sup>27</sup> between the air-related and vapor-related cluster gravity centers in the range of 7–19 un., which makes possible a reliable analyte recognition.

The effect of annealing temperature on the sensing properties of  $\text{Ti}_3\text{C}_2\text{T}_x$  MXene devices is illustrated by [Figure 2](#). Because the multielectrode sensor chip was wire-bonded to a plastic frame ([Figure 1d](#)) that could not withstand temper-

atures higher than 350 °C, we investigated the sensor responses of  $\text{Ti}_3\text{C}_2\text{T}_x$  MXene films in the temperature range from 20 to 350 °C. While the data in [Figure 2](#) are shown for two representative segments on a chip that were tested in experiments with 250 ppm of ethanol, other segments showed similar trends in temperature-dependent sensing experiments for all tested analytes at various concentrations.

[Figure 2a](#) shows an illustrative response of a representative pristine  $\text{Ti}_3\text{C}_2\text{T}_x$  MXene segment to 250 ppm of ethanol at room temperature (20 °C). After a few original analyte–air cycles the sensing responses stabilized, and the device could be cycled multiple times showing a very stable behavior ([Figure 2a](#)). The observed room-temperature responses were consistent with the results of previous sensor studies of metallic  $\text{Ti}_3\text{C}_2\text{T}_x$  MXene and demonstrated the overall high conductivity of films, its decrease in the presence of analyte molecules, and low electrical noise.<sup>14</sup>

[Figure 2b](#) shows the effect of annealing temperature on sensor responses of another segment on a multielectrode chip to 250 ppm of ethanol. The pristine  $\text{Ti}_3\text{C}_2\text{T}_x$  MXene segment measured at room temperature demonstrated a very similar behavior to the segment shown in [Figure 2a](#) with its conductivity decreasing in the presence of the analyte molecules. The initial annealing resulted in degraded sensing properties, and practically no responses to 250 ppm of ethanol were observed when the chip was annealed at 100 °C and then measured at the same temperature; the same was observed for the annealing/measurement temperature of 200 °C ([Figure 2b](#)). Interestingly, the segment started responding to ethanol again upon annealing at 300 °C, although the sensing responses became qualitatively different: while the electrical conductivity decreased upon exposure to ethanol for pristine  $\text{Ti}_3\text{C}_2\text{T}_x$ , it increased for the annealed MXene ([Figure 2b](#)). The conductivity increase in the presence of ethanol molecules was also observed for the same segment when it was annealed and measured at 350 °C ([Figure 2b](#)). While the room temperature data ([Figure 2a,b](#)) show the intrinsic response of metallic  $\text{Ti}_3\text{C}_2\text{T}_x$  MXene that exhibits decreased conductivity in the presence of alcohol molecules,<sup>12,14</sup> we attribute the opposite sensing response in the samples annealed and measured at 300–350 °C to semiconducting TiO<sub>2</sub> nanoparticles that form due to the partial oxidation of  $\text{Ti}_3\text{C}_2\text{T}_x$ . Therefore, negligible sensing responses of the segments that were annealed and measured at intermediate temperatures, such as 100 and 200 °C, can be explained by competing sensing responses of  $\text{Ti}_3\text{C}_2\text{T}_x$  and the TiO<sub>2</sub> nanoparticles.

[Figure 2b](#) shows that the pristine  $\text{Ti}_3\text{C}_2\text{T}_x$  MXene exhibits the largest absolute conductivity change upon exposure to 250 ppm of ethanol compared to the annealed materials. However, the relative conductivity changes are the largest at 350 °C, when upon exposure to 250 ppm of ethanol, the current through the segment at  $V = 1$  V increases by a factor of  $\sim 2$ , from  $\sim 8$  to  $\sim 16$  nA ([Figure 2b](#)). This is further illustrated by [Figure 2c](#), which shows that the sensor response, defined as  $G/G_{\text{air}}$ , where  $G$  is the conductance of the device in the presence of analyte molecules, while  $G_{\text{air}}$  is its conductance in dry air, is the highest for the segment annealed and measured at 350 °C. The highest sensor response at 350 °C is also shown by [Figure 2d](#), which displays  $\Delta G/G_{\text{air}}$  values ( $\Delta G = G - G_{\text{air}}$ ) averaged for multiple analyte–air cycles for the same segment annealed and measured at different temperatures.

In addition to justifying the use of 350 °C as the annealing and measurement temperature, [Figure 2c](#) also shows that high

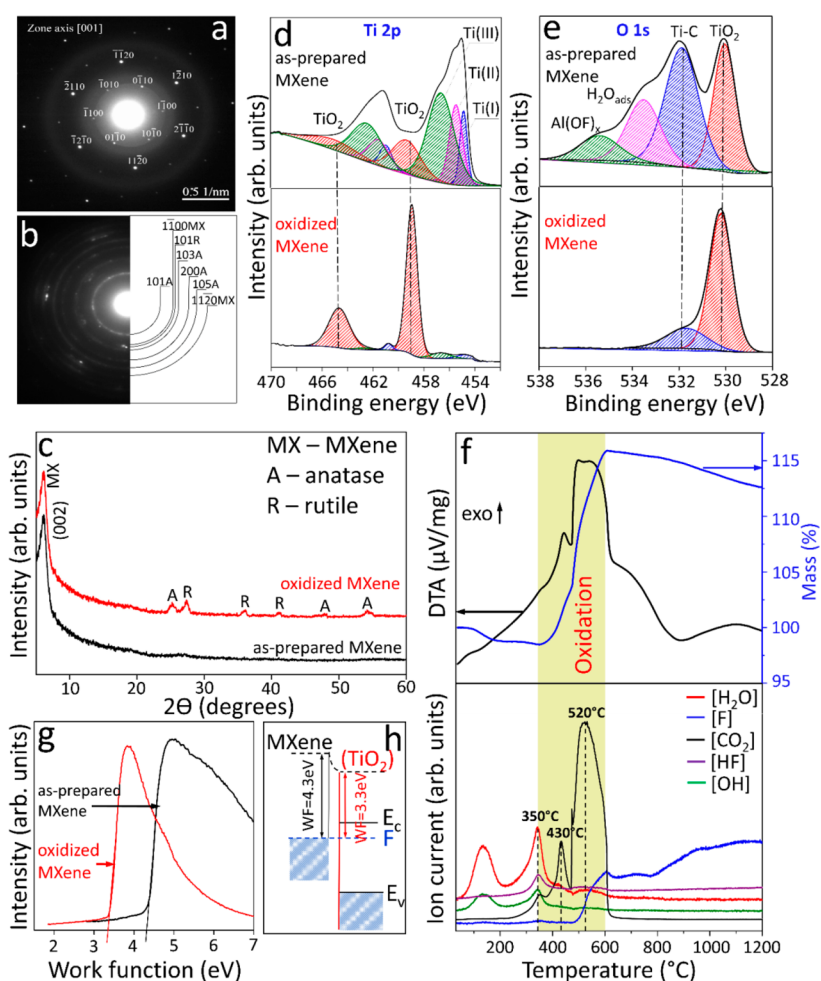


**Figure 3.** Comparison of pristine and partially oxidized MXene materials. (a,b) SAED patterns for MXene flakes (a) before and (b) after oxidation. (c) XRD spectra of MXene powders before and after oxidation. (d) XPS Ti 2p and (e) O 1s spectra of pristine and oxidized MXenes. (f) TGA/DTA-MS analysis of a  $\text{Ti}_3\text{C}_2\text{T}_x$  powder in synthetic air. (g) UPS spectra of MXene before and after oxidation. (h) Energy band diagram of the interface between pristine and oxidized MXene regions based on the UPS data; WF is a work function, F is a Fermi level,  $E_c$  and  $E_v$  are conduction and valence bands, respectively.

temperatures considerably improve the response times of the sensors. In the case of the pristine  $\text{Ti}_3\text{C}_2\text{T}_x$  MXene, upon its exposure to 250 ppm of ethanol at room temperature the conductivity slowly changes over the course of several minutes and then exhibits an even slower recovery upon purging with dry air (Figure 2c). A similar sensor kinetics was reported in previous studies of the pristine  $\text{Ti}_3\text{C}_2\text{T}_x$  MXene.<sup>12,14</sup> At 300 °C, the device responds much faster to the analyte, although in the purging cycles, slow recovery tails can still be observed (Figure 2c). At 350 °C, both conductivity increase (analyte cycle) and recovery (purging cycle) happen on the scale of seconds, showing a much faster response than the pristine  $\text{Ti}_3\text{C}_2\text{T}_x$  MXene at room temperature (Figure 2c).

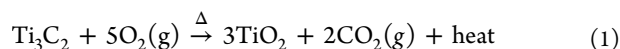
To understand the nature of the observed chemiresistive effect we performed an extensive comparative analysis of the pristine  $\text{Ti}_3\text{C}_2\text{T}_x$  and MXene sheets oxidized by annealing in air at 350 °C; the analytical methods are described in the Experimental Section. First, we performed transmission electron microscopy (TEM) of the pristine and oxidized MXene flakes. TEM analysis of the as-prepared  $\text{Ti}_3\text{C}_2\text{T}_x$  revealed uniform semitransparent flakes (Figure S3) which exhibited well-resolved selected area electron diffraction (SAED) patterns with hexagonal symmetry (Figure 3a). On

the basis of the measured interplanar spacing of 2.66 and 1.54 Å for (1100) and (1120) planes, respectively, we calculated the *a* lattice parameter of 3.056 Å which is in agreement with that of the  $\text{Ti}_3\text{AlC}_2$  MAX phase precursor.<sup>32</sup>

In contrast, the surface and edges of the annealed MXene sheets were decorated with elongated nanoparticles that were 10–40 nm in size (Figure S3). A representative SAED pattern of a partially oxidized MXene flake still shows the diffraction spots corresponding to  $\text{Ti}_3\text{C}_2\text{T}_x$ , but they are accompanied by the spots corresponding to the tetragonal anatase (A) and rutile (R) phases of  $\text{TiO}_2$  (Figure 3b). Similar to the results of TEM and SAED, powder X-ray diffraction (XRD) analysis shows that while  $\text{Ti}_3\text{C}_2\text{T}_x$  mostly survives upon annealing in air at 350 °C, some of the material oxidizes forming a mixture of anatase and rutile. The XRD spectrum of the as-prepared  $\text{Ti}_3\text{C}_2\text{T}_x$  MXene (Figure 3c) confirms the complete etching of the Al layers from  $\text{Ti}_3\text{AlC}_2$ , as the intense (002) basal plane peak shows a characteristic shift to lower angles ( $2\theta = 7^\circ$ ) corresponding to an increased interplanar spacing.<sup>33</sup> While the  $\text{Ti}_3\text{C}_2\text{T}_x$  peak is also the most intense one in the XRD spectrum of the annealed MXene, much smaller peaks corresponding to anatase and rutile phases of  $\text{TiO}_2$  indicate the partial oxidation.

The TEM, SAED, and XRD findings agree well with the X-ray photoelectron spectroscopy (XPS) data (Figure 3d,e, Table S1). The Gaussian–Lorentzian fitting of the XPS Ti 2p<sub>3/2</sub> and Ti 2p<sub>1/2</sub> peaks for the as-prepared MXenes reveals that titanium appears in these structures in four doublets (Ti 2p<sub>3/2</sub>–Ti 2p<sub>1/2</sub>) with a fixed area ratio close to 2:1. The Ti 2p components were fitted as Ti–C, Ti(II), Ti(III) that could be attributed to Ti bound to carbon at binding energy (BE) = 455.1 (461.3) eV and Ti atoms bonded with –O or –OH at BE = 457.1 (462.9) eV and 455.8 (461.6) eV, respectively.<sup>34</sup> In this case, Ti–C, Ti(II), and Ti(III) species constitute the majority fraction (~82%) of the XPS spectrum related to Ti 2p. The Ti 2p<sub>3/2</sub> component centered at 458.9 eV refers to Ti ions with a formal valence of IV (TiO<sub>2</sub>), which forms due to the spontaneous surface oxidation, and comprises only about 18% of that region. The O 1s region in the XPS spectrum of the as-prepared MXenes has been fitted by components corresponding to C–Ti–(OH)<sub>x</sub> at BE = 531.9 eV and strongly adsorbed water at BE = 533.5 eV, which are the majority fractions (~61%) in that spectrum. The balance is in the form of TiO<sub>2</sub> and Al(OF)<sub>x</sub>. Following the oxidation of the MXene flakes, we have observed a significant increase in the Ti 2p peak intensities at 458.9 and 464.5 eV which correspond to TiO<sub>2</sub> 2p<sub>3/2</sub> and TiO<sub>2</sub> 2p<sub>1/2</sub>, respectively. Moreover, the photoemission intensity of the TiO<sub>2</sub> components in the spectra increased by about 86%. Similar changes were observed for the XPS O 1s spectra (Figure 3e) indicating the oxidation of MXene flakes and conversion of their surface termination. Still, the Ti–C bonds in the XPS spectra of oxidized MXenes at 455.0 (461.2) eV remain clearly visible though reduce in intensity.

*In situ* correlative analysis of the annealing of Ti<sub>3</sub>C<sub>2</sub>T<sub>x</sub> from room temperature to 1200 °C in synthetic air using thermal gravimetric (TG) analysis, differential temperature analysis (DTA) and mass spectrometry (MS) of volatile reaction products provides a detailed picture of the MXene oxidation (Figure 3f). First, we observed the water desorption which is evidenced by the broad H<sub>2</sub>O and OH ion current peaks spanning from ~80 to ~200 °C and the corresponding mass loss (Figure 3f). Above ~200 °C, these volatile species are followed by HF and CO<sub>2</sub>, and all four ionic currents show correlated maxima at about 350 °C which are accompanied by a small mass loss (Figure 3f) likely associated with the removal of the remaining adsorbates and some of the surface functionalities. A rapid mass increase at temperatures above ~350 °C manifests active oxidation of MXene in accordance with the net reaction



where an oxidation of 1 mol of Ti<sub>3</sub>C<sub>2</sub> (167.6 g) results in the formation of 3 mol of TiO<sub>2</sub> (3 mol × 79.9 g/mol = 239.7 g). The DTA results show that the Ti<sub>3</sub>C<sub>2</sub> oxidation is an exothermic process; the well-resolved DTA peaks at 430 and 520 °C correlate well with the corresponding CO<sub>2</sub> ion current peaks, see eq 1. The XRD spectrum recorded for the material annealed at 600 °C in air shows a mixture of anatase and rutile reflections and no characteristic peak at 2θ = 7° corresponding to stacked MXene sheets (Figure S4) which confirms the Ti<sub>3</sub>C<sub>2</sub>T<sub>x</sub> oxidation to TiO<sub>2</sub>. Interestingly, the loss of –F surface terminations from MXene becomes most noticeable above ~480 °C and extends through 1200 °C; the F ion current correlates well with a small but steady mass loss at

temperatures above approximately 600 °C. Overall, the results of correlated thermal/MS analysis suggest that 350 °C, which is the onset of active oxidation, is an optimal temperature for annealing of Ti<sub>3</sub>C<sub>2</sub>T<sub>x</sub> films, where most of the MXene material remains in its pristine state to enable good electron transport, and yet a considerable amount of semiconducting TiO<sub>2</sub> is already formed to enhance the chemiresistive properties.

The gas sensing properties of the metal/semiconductor Ti<sub>3</sub>C<sub>2</sub>T<sub>x</sub>/TiO<sub>2</sub> composite films strongly depend on the interfacial properties of the junctions between the pristine and oxidized MXene flakes. The charge carrier transport throughout the network of flakes is governed by the potential barriers between them, while the appeared boundary potentials primarily depend on the difference between the corresponding work functions (WFs) of pristine and oxidized MXenes. Using ultraviolet photoelectron spectroscopy (UPS) we found that WF of the Ti<sub>3</sub>C<sub>2</sub>T<sub>x</sub> MXene dramatically changes upon annealing in air at 350 °C. The as-prepared MXene was found to have WF = 4.4 eV (Figure 3g), which agrees with other experimental observations<sup>35</sup> and was supported by theoretical calculations.<sup>36</sup> Upon oxidation, the work function decreases to 3.3 eV (Figure 3g), so the oxidized structures form a potential barrier with the pristine Ti<sub>3</sub>C<sub>2</sub>T<sub>x</sub> of about 1 eV. According to the band diagram (Figure 3h), the electrons in TiO<sub>2</sub> nanoparticles sink into the conductive MXene channel while the potential barrier prevents the electrons from diffusing back into TiO<sub>2</sub>. Considering the few-nanometer size of the TiO<sub>2</sub> nanoparticles and the estimated Debye length in nonstoichiometric titanium dioxide of about 10 nm,<sup>37</sup> the TiO<sub>2</sub> nanoparticles on the MXene surface are expected to be fully electron-depleted. A similar mechanism of the formation of a depleted layer at the metal–semiconductor interface was proposed for the TiO<sub>2</sub>/MXene composites studied for photocatalytic applications<sup>38</sup> and in the heterojunction that appeared at the interfaces of the Ti<sub>3</sub>C<sub>2</sub> nanosheets and TiO<sub>2</sub> nanowires.<sup>23</sup>

The partially oxidized MXene films produced by annealing in air at 350 °C are less conductive than the pristine Ti<sub>3</sub>C<sub>2</sub>T<sub>x</sub> films tested at room temperature<sup>38</sup> (Figure 2b). This is further evidenced by the increase of the MXene film sheet resistance from 190 Ω/□ to 558 Ω/□ after partial oxidation in air at 350 °C (Figure S5), which is also consistent with recent experimental results reported by Y. Lee et al.<sup>39</sup> At the same time, the linear *I*–*V* curves of MXene film in both cases, before and after annealing, indicate no significant contact degradation. It should be noted that while the increase of resistance was observed upon annealing for all MXene films tested in this study, the magnitude of this increase varied considerably depending on the film thickness and microstructure. On the basis of the UPS data, the decreased conductivity of the annealed MXene films, despite the presence of metallic Ti<sub>3</sub>C<sub>2</sub>T<sub>x</sub> as evidenced by SAED and XRD, can be explained by the fact that the electron depleted TiO<sub>2</sub> nanoparticles form potential barriers between the conductive Ti<sub>3</sub>C<sub>2</sub>T<sub>x</sub> sheets. As the adsorbed analyte molecules dope TiO<sub>2</sub> nanoparticles, a potential barrier lowers and the electrical conductivity of a MXene film improves, which we observe experimentally (Figure 1f). Overall, the experimental results suggest that the enhancement of conductivity of the partially oxidized MXene films in the sensor experiments involves doping of TiO<sub>2</sub> nanoparticles by the adsorbed analyte molecules which is followed by the potential barrier decrease and the corresponding increase in conductivity. The electronic phenomena

occurring at the  $\text{TiO}_2$ /molecule interfaces have been extensively studied experimentally and theoretically<sup>40,41</sup> and are addressed in the Supporting Information. The observations are consistent with high sensor responses that we have experimentally obtained. Furthermore, the simulations do not reveal considerable variations for different phases of  $\text{TiO}_2$ , suggesting that both anatase and rutile nanoparticles could be employed for enhancing the gas sensing properties of  $\text{Ti}_3\text{C}_2\text{T}_x$  MXene.

To quantitatively describe the chemiresistive effect we introduce (see Supporting Information) a sensitivity coefficient,  $\alpha$  ( $\% \text{ ppm}^{-1}$ ), defined as a gas response of a sensor ( $\%$ ) divided by a gas concentration ( $\text{ppm}$ ), which allows us to properly compare our experimental data with the literature results. For isopropyl alcohol, ethanol, methanol, and acetone vapors the  $\alpha$  values are within the 27–50, 11–21, 21–55, and 40–89%  $\text{ppm}^{-1}$  ranges, respectively. These  $\alpha$  values are several orders of magnitude higher than the sensitivity coefficients for graphene oxide of about 0.002%  $\text{ppm}^{-1}$ , which were measured for various alcohols on a similar multisensor chip under similar conditions in our prior study.<sup>40</sup> The sensitivity coefficients for the partially oxidized  $\text{Ti}_3\text{C}_2\text{T}_x$  MXene are comparable with the values reported for gas sensors based on semiconducting nanostructures, such as 5–80%  $\text{ppm}^{-1}$  reported for  $\text{SnO}_2$  nanobelts.<sup>41</sup> The data presented here suggest that the semiconducting  $\text{TiO}_2$  nanoparticles that appear on the surface of MXene upon oxidation are responsible for a high sensitivity, which is greatly enhanced compared to the sensitivity of metallic  $\text{Ti}_3\text{C}_2\text{T}_x$  sheets (Figure S2). The observed differences between the material's gas response to the test analyte vapors could be primarily explained by the interaction of the adsorbed molecules with the sensor's surface, where the number of radicals that appeared upon the dissociation of molecules varied. In principle,  $\text{TiO}_2$  nanoclusters were shown to form on the surface of  $\text{Ti}_3\text{C}_2\text{T}_x$  in air even at room temperature,<sup>42</sup> while annealing at 350 °C increases the amount of  $\text{TiO}_2$ , which was confirmed by SAED, XRD, XPS, and thermal analysis. On the basis of the UPS results and DFT calculations we propose that the observed conductivity increase of the partially oxidized MXene films upon their exposure to molecular analytes is based on the charge transfer from molecules to oxide nanoparticles followed by the reduction of the potential barriers at the  $\text{Ti}_3\text{C}_2\text{T}_x/\text{TiO}_2$  interfaces and the associated enhancement of electrical conductivity.

## CONCLUSIONS

The results of this study demonstrate that partially oxidized  $\text{Ti}_3\text{C}_2\text{T}_x$  MXene can be employed in gas sensors with high chemiresistive responses to organic vapors. The annealed MXene films remain electrically conductive, while their decoration with semiconducting  $\text{TiO}_2$  considerably improves their chemiresistive response to organic analytes at low-ppm concentrations. High sensitivity of the partially oxidized MXene films to organic vapors was observed in dry air, which better emulates practical sensing environments than an inert atmosphere, such as nitrogen. Also, in addition to the low-ppm sensitivity we demonstrated faster sensing responses compared to pristine MXene sensors, as well as selective recognition of analytes of nearly the same chemical nature, such as low molecular weight alcohols, which was achieved by processing sensor data from multiple sensing elements on a multielectrode chip. We investigated the oxidation behavior of  $\text{Ti}_3\text{C}_2\text{T}_x$  in air in a wide temperature range and discussed the

mechanism of sensor response of partially oxidized MXene films, which is qualitatively different from that of pristine  $\text{Ti}_3\text{C}_2\text{T}_x$ . The results of this study demonstrate that partially oxidized MXene films hold great promise for gas sensing applications and warrant further sensor studies of composite nanostructures combining various MXene materials and transition metal oxide nanoparticles.

## EXPERIMENTAL SECTION

**MXene Synthesis.** The  $\text{Ti}_3\text{AlC}_2$  MAX phase was synthesized according to the previously published procedure.<sup>25</sup> In brief, commercial powders of Ti, Al, and TiC were first mixed by ball milling for 24 h to produce a precursor powder with a Ti/Al/C molar ratio of 3.0:1.1:1.9. The mixture was annealed in a corundum crucible at 1400 °C for 2 h under Ar atmosphere using a tube furnace (Carbolite). The obtained MAX compact was crushed and sifted through a stainless steel 400 mesh sieve (Fritsch) to produce a powder with an average particle size of less than 30  $\mu\text{m}$ . To obtain  $\text{Ti}_3\text{C}_2\text{T}_x$  MXene the  $\text{Ti}_3\text{AlC}_2$  MAX precursor was etched in a solution prepared by dissolving 1 g of lithium fluoride (LiF, 99.0%) in 20 mL of 6 M hydrochloric acid (HCl, technical grade) while stirring with a magnetic stir bar in a polypropylene plastic vial for 10 min. One gram of MAX powder was carefully added to the solution at 35 °C and stirred for 24 h. The resulting product was washed with deionized water and centrifuged at 3500 rpm several times until the neutral pH of the supernatant was reached. A multilayer  $\text{Ti}_3\text{C}_2\text{T}_x$  powder was collected by vacuum-assisted filtration through a polyvinylidene difluoride membrane (0.45 mm pore size, Millipore) and dried in vacuum ( $p = 0.15 \text{ Pa}$ ) at 80 °C for 24 h. Then, the filtrate was dispersed in deionized water by ultrasonication at 35 kHz for 1 h (Laborette 17, Fritsch) in order to delaminate the MXene flakes. The resulting solution was centrifuged at 3500 rpm for 1 h to extract single-layer flakes. A 0.5 mg/mL MXene dispersion in deionized water was used for the deposition onto multielectrode chips for electrical measurements.

**MAX Phase and MXene Characterization.** XRD patterns of MAX phase and MXene samples were collected using a Rigaku Miniflex 600 X-ray diffractometer with monochromatic  $\text{Cu K}\alpha$  radiation ( $\lambda = 1.5406 \text{ \AA}$ ). Morphology of the MAX phase powder was investigated by SEM using a TESCAN VEGA 3 instrument. TEM and SAED were performed using a JEOL LEM-1400 transmission electron microscope at the accelerating voltage of 200 kV. AFM was performed using a Digital Instruments Nanoscope IIIa Dimension 3100 system.

Chemical composition of the surfaces of pristine and oxidized MXenes was characterized by XPS using a Kratos Axis Supra spectrometer. Peak fitting was performed using a Gaussian–Lorentzian peak shape after the subtraction of the Shirley background using CasaXPS software (version 2.3.17). All XPS spectra were recorded at the pass energy of 20 eV. The binding energies measured for particular elements were adjusted relative to the C 1s peak (285.0 eV, binding of C–C/ $\text{CH}_x$ ). UPS was carried out on a Kratos Axis Supra spectrometer using a cold cathode UV lamp. Helium was used as a discharge gas in He(1) mode providing a radiation with the energy of 21.22 eV. Spectrometer pass energy was set to 5 eV to obtain a high-energy resolution. No charge neutralization by low energy electrons was applied during the analysis; the sample was biased at the potential of –9 V to ensure the detection of low-energy electrons that are necessary to observe secondary electron cut off. The diameter of the analyzed area was 400  $\mu\text{m}$ , the emission angle between the sample normal and the spectrometer axis was 0°. The work function was calculated by subtracting the secondary electron cutoff energy from the incident ultraviolet photon energy.

The MXene powder sample was studied by a thermal analysis, which included DTA, TGA, and mass spectrometry. The analysis was performed using a Netzsch STA 449 F3 Jupiter instrument coupled with a 403 Aeolos Quadro quadrupole mass spectrometer. The powder was heated in alumina crucibles using a silicon carbide furnace. Prior to the experiments the sample was evacuated; the analysis was performed in synthetic air in the temperature range from

35 to 1200 °C with the heating rate of 10 °C/min. The ion currents corresponding to the mass-to-charge ratios ( $M/Z$ ) of 17, 18, 19, 20, and 44 were recorded.

Sheet resistances of MXene films before and after annealing in air at 350 °C were estimated using an Ecopia HMS-3000 Hall measurement system via van der Pauw method.

**Multisensor Chip.** We utilized a multielectrode chip that contained 39 Pt strip coplanar electrodes on a Si/SiO<sub>2</sub> substrate.<sup>43</sup> The interelectrode distance was about 50 μm, the Pt electrodes were about 4 mm long, 150 μm wide, and 1 μm thick. A droplet of a ~ 0.5 mg/mL aqueous solution of delaminated Ti<sub>3</sub>C<sub>2</sub>T<sub>x</sub> MXene sheets was drop-casted on a substrate and dried in air. The MXene film that formed upon drying bridged 39 Pt electrodes forming 38 sensor devices that could be measured independently of each other. The frontside of the substrate had two meander-shaped Pt thermoresistors at the edges to monitor the operating temperature which was adjusted by four meander heaters located on the backside. The operating temperature was maintained by a KAMINA electronics unit<sup>44</sup> with an accuracy of ±1 °C, while the spatial temperature distribution over the chip substrate was ±10 °C.<sup>27</sup> We tested several multielectrode chips with MXene films; the reported data represents one exemplary chip while others showed very similar behavior in gas sensing experiments.

**Gas Response Measurements.** Sensor measurements of multi-sensor chips covered with partially oxidized MXene films were performed using a setup, which included a home-built data acquisition unit, a purge air generator to establish a dry air background (PG14L, Peak Scientific), and gas delivery tubes. For dosing gas analytes at low concentrations (2–10 ppm), we used a test gas generator based on permeation tubes (OVG-4, Owlstone), while for analytes at concentrations >100 ppm we used capillary diffusion tubes, as described in our previous works.<sup>4,40,45</sup> A data acquisition module (National Instruments USB-6259) together with a current preamplifier (SRS, SR570) were used to measure resistances of all chemiresistive elements on a chip.<sup>46</sup> To read out the entire array of devices we employed a multiplexing card for switching between the chemiresistive elements on a chip. Organic vapors of the same reducing nature, alcohols (methanol, ethanol, isopropyl alcohol) and acetone, were utilized as test analytes at ppm concentrations, which were controlled by the heating temperature of permeation tubes. The devices were exposed to organic vapors during 10 min intervals, which were separated by pulses of dry air that lasted 10–25 min to ensure the recovery of the chip segment resistances. The lowest concentration available for all four vapors under the normal operation of a gas generator was 2 ppm. Higher concentrations of vapors in mixtures with dry air were 5 and 10 ppm. All gases were supplied in a flow mode at the 100 sccm rate. The maximum operating temperature was 350 °C. The gas response was defined as the change in the conductance upon gas injection compared to the baseline conductance in dry air ( $S = G/G_{\text{air}}$ ). The gas sensitivity coefficients employed to compare the obtained data with the available literature results were calculated as  $S/C$ , where  $C$  is the gas concentration (ppm).

## ■ ASSOCIATED CONTENT

### SI Supporting Information

The Supporting Information is available free of charge at <https://pubs.acs.org/doi/10.1021/acsnm.9b02223>.

Additional information about the composition of Ti<sub>3</sub>AlC<sub>2</sub> MAX phase, comparison of gas response data for MXenes, TEM images of as-prepared and oxidized Ti<sub>3</sub>C<sub>2</sub>T<sub>x</sub> MXenes, XRD pattern of Ti<sub>3</sub>C<sub>2</sub>T<sub>x</sub> MXene after oxidation, XPS peak fittings for as-prepared and oxidized MXenes, anatase and rutile structures, and electron density distributions in TiO<sub>2</sub> under adsorption of alcohol molecules (PDF)

## ■ AUTHOR INFORMATION

### Corresponding Authors

**Hanna Pazniak** – Department of Functional Nanosystems and High-Temperature Materials, National University of Science and Technology “MISiS”, Moscow 119049, Russia;

[orcid.org/0000-0002-0592-9009](https://orcid.org/0000-0002-0592-9009); Email: [hanna.pazniak@univ-poitiers.fr](mailto:hanna.pazniak@univ-poitiers.fr)

**Victor V. Sysoev** – Department of Physics, Yuri Gagarin State Technical University of Saratov, Saratov 410054, Russia;

[orcid.org/0000-0002-0372-1802](https://orcid.org/0000-0002-0372-1802); Email: [vsysoev@sstu.ru](mailto:vsysoev@sstu.ru)

**Alexander Sinitskii** – Department of Chemistry, University of Nebraska-Lincoln, Lincoln, Nebraska 68588, United States;

[orcid.org/0000-0002-8688-3451](https://orcid.org/0000-0002-8688-3451); Email: [sinitskii@unl.edu](mailto:sinitskii@unl.edu)

### Authors

**Ilya A. Plugin** – Department of Physics, Yuri Gagarin State Technical University of Saratov, Saratov 410054, Russia

**Michael J. Loes** – Department of Chemistry, University of Nebraska-Lincoln, Lincoln, Nebraska 68588, United States

**Talgat M. Inerbaev** – V. S. Sobolev Institute of Geology and Mineralogy SB RAS, Novosibirsk 630090, Russia; L. N. Gumilyov Eurasian National University, Astana 010008, Kazakhstan

**Igor N. Burmistrov** – Department of Functional Nanosystems and High-Temperature Materials, National University of Science and Technology “MISiS”, Moscow 119049, Russia; Engineering Center, Department of Chemistry of Innovative Materials and Technologies, Plekhanov Russian University of Economics, Moscow 117997, Russia

**Michail Gorshenkov** – Department of Functional Nanosystems and High-Temperature Materials, National University of Science and Technology “MISiS”, Moscow 119049, Russia

**Josef Polcak** – CEITEC-Central European Institute of Technology and Institute of Physical Engineering, Brno University of Technology, Brno 61600, Czech Republic

**Alexey S. Varezchnikov** – Department of Physics, Yuri Gagarin State Technical University of Saratov, Saratov 410054, Russia

**Martin Sommer** – Institute of Microstructure Technology, Karlsruhe Institute of Technology, Eggenstein-Leopoldshafen 76344, Germany

**Denis V. Kuznetsov** – Department of Functional Nanosystems and High-Temperature Materials, National University of Science and Technology “MISiS”, Moscow 119049, Russia

**Michael Bruns** – Institute for Applied Materials, Karlsruhe Institute of Technology (KIT), Eggenstein-Leopoldshafen 76344, Germany

**Fedor S. Fedorov** – Skolkovo Institute of Science and Technology, Moscow 121205, Russia

**Natalia S. Vorobeva** – Department of Chemistry, University of Nebraska-Lincoln, Lincoln, Nebraska 68588, United States

Complete contact information is available at:

<https://pubs.acs.org/doi/10.1021/acsnm.9b02223>

### Notes

The authors declare no competing financial interest.

## ■ ACKNOWLEDGMENTS

The work was carried out with the financial support from the Ministry of Education and Science of the Russian Federation in the framework of the Increase Competitiveness Program of NUST “MISiS” (No. K4-2017-043), implemented by the government decree from 16th of March 2013, N 211. I.A.P.,

A.S.V., and V.V.S. thank the Ministry of Education and Science of the Russian Federation for their support by Grant No. 16.1119.2017/4.6. The work of T.M.I. was performed under the state assignment of IGM SB RAS. T.M.I. also thanks the Center for Computational Materials Science (IMR, Tohoku University) for access to the supercomputing system to perform the simulations. The calculations were partially performed at the Cherry supercomputer cluster provided by the Materials Modeling and Development Laboratory at NUST "MISIS" (supported via the Grant from the Ministry of Education and Science of the Russian Federation No. 14.Y26.31.0005). A.S. thanks the Nebraska Center for Energy Sciences Research for support. J.P. gratefully acknowledges CzechNanoLab Research Infrastructure supported by MEYS CR (LM2018110) and the project CEITEC 2020 (LQ1601) supported by MEYS CR under the National Sustainability Programme II.

## REFERENCES

- (1) Yang, S.; Jiang, C.; Wei, S.-H. Gas Sensing in 2D materials. *Appl. Phys. Rev.* **2017**, *4*, 021304.
- (2) Schedin, F.; Geim, A. K.; Morozov, S. V.; Hill, E. W.; Blake, P.; Katsnelson, M. I.; Novoselov, K. S. Detection of Individual Gas Molecules Adsorbed on Graphene. *Nat. Mater.* **2007**, *6*, 652–5.
- (3) Varghese, S. S.; Lonkar, S.; Singh, K. K.; Swaminathan, S.; Abdala, A. Recent Advances in Graphene Based Gas Sensors. *Sens. Actuators, B* **2015**, *218*, 160–183.
- (4) Mehdi Pour, M.; Lashkov, A.; Radocea, A.; Liu, X.; Sun, T.; Lipatov, A.; Korlacki, R. A.; Shekhirev, M.; Aluru, N. R.; Lyding, J. W.; Sysoev, V.; Sinitiskii, A. Laterally Extended Atomically Precise Graphene Nanoribbons with Improved Electrical Conductivity for Efficient Gas Sensing. *Nat. Commun.* **2017**, *8*, 820.
- (5) Fowler, J. D.; Allen, M. J.; Tung, V. C.; Yang, Y.; Kaner, R. B.; Weiller, B. H. Practical Chemical Sensors from Chemically Derived Graphene. *ACS Nano* **2009**, *3*, 301–306.
- (6) Late, D. J.; Huang, Y.-K.; Liu, B.; Acharya, J.; Shirodkar, S. N.; Luo, J.; Yan, A.; Charles, D.; Waghmare, U. V.; Dravid, V. P.; Rao, C. N. R. Sensing Behavior of Atomically Thin-Layered MoS<sub>2</sub> Transistors. *ACS Nano* **2013**, *7*, 4879–4891.
- (7) Huo, N.; Yang, S.; Wei, Z.; Li, S.-S.; Xia, J.-B.; Li, J. Photoresponsive and Gas Sensing Field-Effect Transistors based on Multilayer WS<sub>2</sub> Nanoflakes. *Sci. Rep.* **2015**, *4*, 5209.
- (8) Cui, S.; Pu, H.; Wells, S. A.; Wen, Z.; Mao, S.; Chang, J.; Hersam, M. C.; Chen, J. Ultrahigh Sensitivity and Layer-dependent Sensing Performance of Phosphorene-based Gas Sensors. *Nat. Commun.* **2015**, *6*, 8632.
- (9) Ji, F.; Ren, X.; Zheng, X.; Liu, Y.; Pang, L.; Jiang, J.; Liu, S. 2D-MoO<sub>3</sub> Nanosheets for Superior Gas Sensors. *Nanoscale* **2016**, *8*, 8696–8703.
- (10) Yu, X.-F.; Li, Y.-C.; Cheng, J.-B.; Liu, Z.-B.; Li, Q.-Z.; Li, W.-Z.; Yang, X.; Xiao, B. Monolayer Ti<sub>3</sub>CO<sub>2</sub>: A Promising Candidate for NH<sub>3</sub> Sensor or Capturer with High Sensitivity and Selectivity. *ACS Appl. Mater. Interfaces* **2015**, *7*, 13707–13713.
- (11) Xiao, B.; Li, Y.-C.; Yu, X.-F.; Cheng, J.-B. MXenes: Reusable Materials for NH<sub>3</sub> Sensor or Capturer by Controlling the Charge Injection. *Sens. Actuators, B* **2016**, *235*, 103–109.
- (12) Lee, E.; VahidMohammadi, A.; Prorok, B. C.; Yoon, Y. S.; Beidaghi, M.; Kim, D.-J. Room Temperature Gas Sensing of Two-Dimensional Titanium Carbide (MXene). *ACS Appl. Mater. Interfaces* **2017**, *9*, 37184–37190.
- (13) Yuan, W.; Yang, K.; Peng, H.; Li, F.; Yin, F. A Flexible VOCs Sensor Based on a 3D MXene Framework with a High Sensing Performance. *J. Mater. Chem. A* **2018**, *6*, 18116–18124.
- (14) Kim, S.-J.; Koh, H.-J.; Ren, C. E.; Kwon, O.; Maleski, K.; Cho, S.-Y.; Anasori, B.; Kim, C.-K.; Choi, Y.-K.; Kim, J.; Gogotsi, Y.; Jung, H.-T. Metallic Ti<sub>3</sub>C<sub>2</sub>T<sub>x</sub> MXene Gas Sensors with Ultrahigh Signal-to-Noise Ratio. *ACS Nano* **2018**, *12*, 986–993.
- (15) Yang, Z.; Liu, A.; Wang, C.; Liu, F.; He, J.; Li, S.; Wang, J.; You, R.; Yan, X.; Sun, P.; Duan, Y.; Lu, G. Improvement of Gas and Humidity Sensing Properties of Organ-like MXene by Alkaline Treatment. *ACS Sens.* **2019**, *4*, 1261–1269.
- (16) Koh, H.-J.; Kim, S. J.; Maleski, K.; Cho, S.-Y.; Kim, Y.-J.; Ahn, C. W.; Gogotsi, Y.; Jung, H.-T. Enhanced Selectivity of MXene Gas Sensors through Metal Ion Intercalation: In Situ X-ray Diffraction Study. *ACS Sens.* **2019**, *4*, 1365–1372.
- (17) Chae, Y.; Kim, S. J.; Cho, S.-Y.; Choi, J.; Maleski, K.; Lee, B.-J.; Jung, H.-T.; Gogotsi, Y.; Lee, Y.; Ahn, C. W. An Investigation into the Factors Governing the Oxidation of Two-dimensional Ti<sub>3</sub>C<sub>2</sub> MXene. *Nanoscale* **2019**, *11*, 8387–8393.
- (18) Ghidui, M.; Lukatskaya, M. R.; Zhao, M.-Q.; Gogotsi, Y.; Barsoum, M. W. Conductive Two-dimensional Titanium Carbide 'clay' with High Volumetric Capacitance. *Nature* **2014**, *516*, 78.
- (19) Naguib, M.; Mochalin, V. N.; Barsoum, M. W.; Gogotsi, Y. 25th Anniversary Article: MXenes: A New Family of Two-Dimensional Materials. *Adv. Mater.* **2014**, *26*, 992–1005.
- (20) Lipatov, A.; Alhabeab, M.; Lukatskaya, M. R.; Boson, A.; Gogotsi, Y.; Sinitiskii, A. Effect of Synthesis on Quality, Electronic Properties and Environmental Stability of Individual Monolayer Ti<sub>3</sub>C<sub>2</sub> MXene Flakes. *Adv. Electron. Mater.* **2016**, *2*, 1600255.
- (21) Korotcenkov, G.; Sysoev, V. Conductometric Metal Oxide Gas Sensors: Principles of Operation and Approaches to Fabrication. In *Chemical Sensors: Comprehensive Sensor Technologies*; Korotcenkov, G., Ed.; Momentum Press: New York, 2011; pp 53–186.
- (22) Tai, H.; Duan, Z.; He, Z.; Li, X.; Xu, J.; Liu, B.; Jiang, Y. Enhanced Ammonia Response of Ti<sub>3</sub>C<sub>2</sub>T<sub>x</sub> Nanosheets Supported by TiO<sub>2</sub> Nanoparticles at Room Temperature. *Sens. Actuators, B* **2019**, *298*, 126874.
- (23) Li, N.; Jiang, Y.; Zhou, C.; Xiao, Y.; Meng, B.; Wang, Z.; Huang, D.; Xing, C.; Peng, Z. High Performance Humidity Sensor Based on Urchin-like Composite of Ti<sub>3</sub>C<sub>2</sub> MXene-derived TiO<sub>2</sub> Nanowires. *ACS Appl. Mater. Interfaces* **2019**, *11*, 38116–38125.
- (24) van den Broek, J.; Abegg, S.; Pratsinis, S. E.; Guentner, A. T. Highly selective detection of methanol over ethanol by a handheld gas sensor. *Nat. Commun.* **2019**, *10*, 4220.
- (25) Alhabeab, M.; Maleski, K.; Anasori, B.; Lelyukh, P.; Clark, L.; Sin, S.; Gogotsi, Y. Guidelines for Synthesis and Processing of Two-Dimensional Titanium Carbide (Ti<sub>3</sub>C<sub>2</sub>T<sub>x</sub> MXene). *Chem. Mater.* **2017**, *29*, 7633–7644.
- (26) Lipatov, A.; Lu, H.; Alhabeab, M.; Anasori, B.; Gruverman, A.; Gogotsi, Y.; Sinitiskii, A. Elastic Properties of 2D Ti<sub>3</sub>C<sub>2</sub>T<sub>x</sub> MXene Monolayers and Bilayers. *Sci. Adv.* **2018**, *4*, No. eaat0491.
- (27) Sysoev, V. V.; Kiselev, I.; Frietsch, M.; Goschnick, J. Temperature Gradient Effect on Gas Discrimination Power of a Metal-Oxide Thin-Film Sensor Microarray. *Sensors* **2004**, *4*, 37–46.
- (28) Chen, W. Y.; Jiang, X.; Lai, S.-N.; Peroulis, D.; Stanciu, L. Nanohybrids of a MXene and Transition Metal Dichalcogenide for Selective Detection of Volatile Organic Compounds. *Nat. Commun.* **2020**, *11*, 1302.
- (29) Henrion, R.; Henrion, G. *Multivariate Datenanalyse*; Springer-Verlag: Berlin, 1995; p 264.
- (30) Jurs, P. C.; Bakken, G. A.; McClelland, H. E. Computational Methods for the Analysis of Chemical Sensor Array Data from Volatile Analytes. *Chem. Rev.* **2000**, *100*, 2649.
- (31) Albert, K. J.; Lewis, N. S.; Schauer, C. L.; Sotzing, G. A.; Stitzel, S. E.; Vaid, T. P.; Walt, D. R. Cross-Reactive Chemical Sensor Arrays. *Chem. Rev.* **2000**, *100*, 2595.
- (32) Lane, N. J.; Vogel, S. C.; Caspi, E. N.; Barsoum, M. W. High-temperature Neutron Diffraction and First-principles Study of Temperature-dependent Crystal Structures and Atomic Vibrations in Ti<sub>3</sub>AlC<sub>2</sub>, Ti<sub>2</sub>AlC, and Ti<sub>3</sub>Al<sub>2</sub>C<sub>3</sub>. *J. Appl. Phys.* **2013**, *113*, 183519.
- (33) Hong Ng, V. M.; Huang, H.; Zhou, K.; Lee, P. S.; Que, W.; Xu, J. Z.; Kong, L. B. Recent Progress in Layered Transition Metal Carbides and/or Nitrides (MXenes) and Their Composites: Synthesis and Applications. *J. Mater. Chem. A* **2017**, *5*, 3039–3068.
- (34) Halim, J.; Cook, K. M.; Naguib, M.; Eklund, P.; Gogotsi, Y.; Rosen, J.; Barsoum, M. W. X-ray Photoelectron Spectroscopy of

Select Multi-layered Transition Metal Carbides (MXenes). *Appl. Surf. Sci.* **2016**, *362*, 406–417.

(35) Zhang, C.; Anasori, B.; Seral-Ascaso, A.; Park, S.-H.; McEvoy, N.; Shmeliov, A.; Duesberg, G. S.; Coleman, J. N.; Gogotsi, Y.; Nicolosi, V. Transparent, Flexible, and Conductive 2D Titanium Carbide (MXene) Films with High Volumetric Capacitance. *Adv. Mater.* **2017**, *29*, 1702678.

(36) Khazaei, M.; Arai, M.; Sasaki, T.; Ranjbar, A.; Liang, Y.; Yunoki, S. OH-terminated Two-dimensional Transition Metal Carbides and Nitrides as Ultralow Work Function Materials. *Phys. Rev. B: Condens. Matter Mater. Phys.* **2015**, *92*, 075411.

(37) Sysoev, V. V.; Button, B. K.; Wepsiec, K.; Dmitriev, S.; Kolmakov, A. Toward the Nanoscopic “Electronic Nose”: Hydrogen vs Carbon Monoxide Discrimination with an Array of Individual Metal Oxide Nano- and Mesowire Sensors. *Nano Lett.* **2006**, *6*, 1584–1588.

(38) Wang, H.; Peng, R.; Hood, Z. D.; Naguib, M.; Adhikari, S. P.; Wu, Z. Titania Composites with 2D Transition Metal Carbides as Photocatalysts for Hydrogen Production under Visible-Light Irradiation. *ChemSusChem* **2016**, *9*, 1490–7.

(39) Lee, Y.; Kim, S. J.; Kim, Y.-J.; Lim, Y.; Chae, Y.; Lee, B.-J.; Kim, Y.-T.; Han, H.; Gogotsi, Y.; Ahn, C. W. Oxidation-Resistant Titanium Carbide MXene Films. *J. Mater. Chem. A* **2020**, *8*, 573–581.

(40) Lipatov, A.; Varezchnikov, A.; Wilson, P.; Sysoev, V.; Kolmakov, A.; Sinitiskii, A. Highly Selective Gas Sensor Arrays Based on Thermally Reduced Graphene Oxide. *Nanoscale* **2013**, *5*, 5426–34.

(41) Sysoev, V. V.; Goschnick, J.; Schneider, T.; Strelcov, E.; Kolmakov, A. A Gradient Microarray Electronic Nose Based on Percolating SnO<sub>2</sub> Nanowire Sensing Elements. *Nano Lett.* **2007**, *7*, 3182–8.

(42) Chertopalov, S.; Mochalin, V. N. Environment-Sensitive Photoresponse of Spontaneously Partially Oxidized Ti<sub>3</sub>C<sub>2</sub> MXene Thin Films. *ACS Nano* **2018**, *12*, 6109–6116.

(43) Fedorov, F. S.; Varezchnikov, A. S.; Kiselev, I.; Kolesnichenko, V. V.; Burmistrov, I. N.; Sommer, M.; Fuchs, D.; Kübel, C.; Gorokhovskiy, A. V.; Sysoev, V. V. Potassium Polytitanate Gas-sensor Study by Impedance Spectroscopy. *Anal. Chim. Acta* **2015**, *897*, 81–86.

(44) Goschnick, J. An Electronic Nose for Intelligent Consumer Products Based on a Gas Analytical Gradient Microarray. *Microelectron. Eng.* **2001**, *57–58*, 693–704.

(45) Shekhirev, M.; Lipatov, A.; Torres, A.; Vorobeva, N. S.; Harkleroad, A.; Lashkov, A.; Sysoev, V.; Sinitiskii, A. Highly Selective Gas Sensors Based on Graphene Nanoribbons Grown by Chemical Vapor Deposition. *ACS Appl. Mater. Interfaces* **2020**, *12*, 7392–7402.

(46) Fedorov, F.; Vasilkov, M.; Lashkov, A.; Varezchnikov, A.; Fuchs, D.; Kübel, C.; Bruns, M.; Sommer, M.; Sysoev, V. Toward New Gas-Analytical Multisensor Chips Based on Titanium Oxide Nanotube Array. *Sci. Rep.* **2017**, *7*, 9732.